DOI: 10.2352/ISSN.2470-1173.2016.18.DPMI-030

Multi-Image Sparse Motion-Invariant Photography

Bart Kofoed [a,b]***, Eric Janssen*** [b] ***and Peter H.N. de With*** [a]
[a] ***Eindhoven University of Technology, Den Dolech 2, 5612 AZ, Eindhoven, The Netherlands***
[b] ***Prodrive Technologies B.V., Science Park Eindhoven 5501, 5692 EM, Son***

Abstract

In this paper we describe and verify a method, called SMIP, to circumvent the trade-off between motion blur and noise, specifically for scenes with predominantly two distinct linear motions (sparse motion). This is based on employing image stabilization hardware to track objects during exposure while capturing two images in quick succession. The two images are combined into a single sharp image without segmentation or local motion estimation. We provide a theoretical analysis and simulations to show that the Signal-to-Noise Ratio (SNR) increases up to 20 dB over conventional short-exposure photography. We demonstrate that the proposed method significantly improves the SNR compared to existing methods. Furthermore, we evaluate a proof-of-concept using modified off-the-shelf optical image stabilization hardware to verify the effectiveness of our method in practice, showing a good correspondence between the simulation and practical results.

Introduction

Photography in dim light, such as in surveillance applications, is commonly limited by the trade-offs of the *exposure triangle*. The exposure triangle relates the three main exposure parameters: exposure time, lens aperture and sensitivity (ISO). Adjusting one parameter implies adjusting at least one of the other two, to maintain a proper exposure. A smaller lens aperture or shorter exposure time decreases defocus- and motion blur, but reduces the light throughput at the same time. On the other hand, compensating with a higher ISO increases the noise level, resulting in a grainy image. Hence, the photographer has to find a suitable trade-off between defocus blur, motion blur and noise.

In this paper we describe and verify a method to circumvent the trade-off between motion blur and noise, specifically for scenes with predominantly two distinct linear motions (sparse motion). A typical example is a traffic surveillance camera with vehicles passing by at high speed. Our method shifts the lens to move the camera viewing direction during the exposure in order to stabilize object motion. Whereas one image is captured while stabilizing one velocity, the second image is stabilized for the other. Both images are combined into an entirely sharp image without the need for local motion estimation (motion-invariant). This explains the name Sparse Motion-Invariant Photography (SMIP).

Our work builds upon Levin *et al.* [1], who have introduced *Motion-Invariant Photography* (MIP). MIP employs constantly accelerating linear camera motion to uniformly blur all objects moving within a range of velocities. Deblurring yields a blur-free image without the need for local blur estimation. MIP allows to increase the exposure time while preventing motion blur, thereby easing the trade-off between motion blur and noise. However, MIP suffers from the following practical limitations.

1. Only a single linear motion direction is stabilized. Although Levin *et al.* have shown that other motion directions can be deblurred as well, it introduces severe artefacts.
2. Ghosting artefacts arise due to the approximate motion-invariance. A motion-independent blur is assumed, while the actual blur function *does* depend on the object velocity.
3. Deblurring amplifies noise as shown by Agrawal and Raskar [2], largely canceling the quality improvements of the longer exposure period. Modern image sensors continue to pursue *shot-noise limited* quality [3], which, together with deblurring noise amplification, almost completely cancels image quality improvements [4].

Let us first discuss prior work before detailing the difference between the main approaches.

Prior work

Circumventing the limits of the exposure triangle has been broadly studied. More recently, *Computational Imaging* (CI) is an emerging field of research focusing on enhanced camera performance and functionality, using a combination of modified optics and post-processing.

Raskar *et al.* [5] introduced *Coded Exposure* (CE), which uses a temporally modulated shutter and subsequent deblurring to obtain sharp images of moving subjects while extending the exposure time. CE does not pose restrictions on the direction of motion, but does require complex image segmentation in post-processing.

Levin *et al.* presented Motion-Invariant Photography. As discussed in the introduction, MIP uses camera motion and subsequent deblurring, to obtain a sharp image without the need for segmentation during post-processing. McCloskey *et al.* has demonstrated an implementation using optical image stabilization hardware [6] and suggested several improvements of both the camera motion [8] and deblurring [7]. Furthermore, Cho *et al.* extended MIP to arbitrary two-dimensional motion [9]. Although both MIP and CE allow for extended exposure periods, Cossairt *et al.* [4] showed that both techniques offer little to no image quality improvement, due to the combined effects of signal-dependent noise and deblurring noise amplification.

Defocus blur can be removed as well, for which several CI techniques have been proposed. They use coded apertures [10], aspherical optics [11], focus stacks [12, 13] or focal sweeping [14, 15]. Defocus deblurring is closely related to motion deblurring. For example, coded aperture- and coded exposure photography both use optical coding to make the blur function invertible. Moreover, focal sweeping and motion-invariant photography both rely on making the blur function independent of depth and motion, respectively.

DOI: 10.2352/ISSN.2470-1173.2016.18.DPMI-030

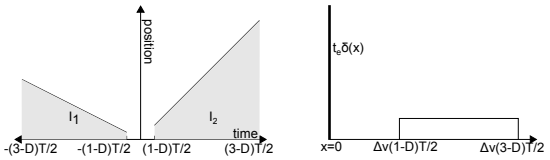

(a) Camera motion trajectory (b) 1-dimensional PSF $\phi(x)$

Figure 1: Camera motion (a) and point spread function (b)

Consider the aforementioned trade-offs, the proposed SMIP reduces noise amplification during deblurring, which significantly improves the image quality. Furthermore, the blur function is identical for both velocities which prevents ghosting artefacts. However, our proposed method does trade-off flexibility for the improved performance when compared to MIP. Whereas MIP handles a continuous range of one-dimensional object velocities, SMIP can only cope with 2 distinct velocities in a scene. Both velocities need to be known in advance, but motion estimation is a mature technology.

Sparse motion-invariant photography

The key assumption for SMIP is that objects in the field-of-view of a camera move at a constant linear two-dimensional velocity, either $\mathbf{v}_1$ or $\mathbf{v}_2$ with $\mathbf{v}_2 > \mathbf{v}_1$. Their relative positions are given by $\mathbf{x}_1(t) = \mathbf{v}_1 t$ and $\mathbf{x}_2(t) = \mathbf{v}_2 t$, respectively, where t denotes time. The camera system is equipped with a mechanism to shift the field-of-view and stabilizes one velocity at a time. Two images I_1 and I_2 are captured in quick succession with sampling period T. The camera shutter opens at a duty cycle D, hence the exposure time for each image is $t_e = D \cdot T$. In practice, $D < 1$ due to camera overhead. Image I_1 is stabilized for $\mathbf{v}_1$, while I_2 is stabilized for $\mathbf{v}_2$.

Motion model

We define the two-dimensional camera field-of-view motion trajectory $\mathbf{x}_c(t)$, as illustrated in Figure 1a, by:

$$\mathbf{x}_c(t) = \begin{cases} \mathbf{v}_1 t & \text{if } t < 0, \\ \mathbf{v}_2 t & \text{if } t > 0. \end{cases} \tag{1}$$

As a result, the motion trajectory of $\mathbf{v}_1$, as seen by the camera, equals $\mathbf{x}_{1,c}(t) = \mathbf{x}_1(t) - \mathbf{x}_c(t)$, which is specified by:

$$\mathbf{x}_{1,c}(t) = \begin{cases} \mathbf{0} & \text{if } t < 0, \\ (\mathbf{v}_1 - \mathbf{v}_2)t & \text{if } t > 0. \end{cases} \tag{2}$$

Similarly, we derive the trajectory of $\mathbf{v}_2$ as seen by the camera, by:

$$\mathbf{x}_{2,c}(t) = \begin{cases} (\mathbf{v}_2 - \mathbf{v}_1)t & \text{if } t < 0, \\ \mathbf{0} & \text{if } t > 0. \end{cases} \tag{3}$$

From the above, we observe two aspects:

- The two motion trajectories as seen by the camera are reversed in time such that $\mathbf{x}_{2,c}(t) = \mathbf{x}_{1,c}(-t)$. This implies that objects moving at $\mathbf{v}_1$ and $\mathbf{v}_2$ are blurred identically.
- Both $\mathbf{x}_{1,c}(t)$ and $\mathbf{x}_{2,c}(t)$ are one-dimensional motion trajectories along the vector $\mathbf{v}_1 - \mathbf{v}_2$, resulting in one-dimensional motion blur.

Point spread function

The Point Spread Function (PSF) describes the projection of a point source on the image sensor. Under the condition that the appearance of an object remains unchanged during the exposure, the PSF is defined by the amount of time spent on a pixel position. If the camera is tracking an object, the PSF becomes a delta impulse function, while the PSF of objects moving at the other velocity becomes a one-dimensional box filter.

Recalling that the motion trajectories $\mathbf{x}_{1,c}(t)$ and $\mathbf{x}_{1,c}(t)$, as seen by the camera, move along the vector $\mathbf{v}_1 - \mathbf{v}_2$, we denote the one-dimensional PSF projected on this vector as $\phi(x)$. In practice, the actual PSF is simply a rotated version of the horizontal $\phi(x)$ function.

For ease of notation, we define $\Delta v = \|\mathbf{v}_2 - \mathbf{v}_1\|$. Let $\phi_{i,j}(x)$ denote the PSF of objects with velocity $\mathbf{v}_i$ in image I_j. Recalling that $\mathbf{x}_{1,c}(t) = \mathbf{x}_{2,c}(t)$, then $\phi_{1,1}(x) = \phi_{2,2}(x)$ and $\phi_{1,2}(x) = \phi_{2,1}(x)$, so that the following holds:

$$\phi_{1,1}(x) = \phi_{2,2}(x) = t_e \delta(x), \tag{4}$$

and similarly we find that:

$$\phi_{1,2}(x) = \phi_{2,1}(x) = \begin{cases} \frac{1}{\Delta v} & \text{if } \Delta v(1-D)\frac{T}{2} \le x \le \Delta v(3-D)\frac{T}{2}, \\ 0 & \text{otherwise.} \end{cases} \tag{5}$$

Adding both images $I = I_1 + I_2$ yields an image in which $\mathbf{v}_1$ is blurred by PSF $\phi_1(x)$ and $\mathbf{v}_2$ by $\phi_2(x)$, where:

$$\phi(x) = \phi_{1,1}(x) + \phi_{1,2}(x) = \phi_{2,1}(x) + \phi_{2,2}(x). \tag{6}$$

A digital image sensor samples light intensity on a grid of square pixels, therefore we use the discrete PSF $h[n]$, defined by integrating PSF $\phi(x)$ over one pixel surface, finally leading to:

$$h[n] = \begin{cases} t_e & \text{if } n = 0 \\ \frac{1}{\Delta v} & \text{if } \Delta v(1-D)\frac{T}{2} \le n \le \Delta v(3-D)\frac{T}{2}, \\ 0 & \text{otherwise.} \end{cases} \tag{7}$$

Finally, using the inverse filter $h_i[n]$, as will be introduced in the next section, the sharp image I_s is computed from I_1 and I_2 by convolution:

$$I_s = (I_1 + I_2) * h_i. \tag{8}$$

Multi-image versus single image

Since only the sum of the two images I_1 and I_2 is used during post-processing, it is also possible to capture a single image while stabilizing $\mathbf{v}_1$ during the first half of the exposure and $\mathbf{v}_2$ during the second half. The advantages are zero camera overhead (D=1), no accumulation of read noise and smaller data storage. A practical issue is that mechanical motion actuators have a finite bandwidth and cannot execute the abrupt change of velocity. Actuator position feedback [8] is necessary to obtain the exact PSF for deblurring. Our hardware lacks position feedback, therefore we resort to the multi-image approach.

Noise

In this section we derive a model for the noise level in the final image I_s. Image noise is introduced by the image sensor and is further amplified during deconvolution. Both factors are taken into account in the following analysis.

DOI: 10.2352/ISSN.2470-1173.2016.18.DPMI-030

Camera noise model

Image sensors suffer from various types of noise [3]. We model image sensor noise as a combination of the following independent noise sources.

1. Read noise: The combined effects of signal-independent noise sources are modelled by a spatially-independent Gaussian distribution with variance σ_r^2.
2. Shot noise: Shot noise results from the random nature of photons arriving on the detector. Let J denote the average scene illumination level, measured in photon interactions per second per pixel. If the average number of photons per detector Jt_e is significantly larger than unity, shot noise is approximated by a Gaussian distribution with variance equal to the signal level Jt_e.
3. Fixed pattern noise: Fixed pattern noise (FPN), or Photo Response Non-Uniformity (PRNU), refers to temporally constant noise caused by spatially non-uniform pixel sensitivity. The noise variance due to FPN is given by $\sigma_{FPN}^2 = P_N^2 J^2 t_e^2$, where P_N denotes the FPN quality factor.

Furthermore, pixels accumulate charge even in the absence of interacting photons. The so-called dark current is mainly thermally generated [3] and results in both fixed-pattern noise and shot-noise. We define the dark current rate D_R in electrons per second, depending on the sensor temperature, which we assume to be constant. Consequently, the noise model includes two additional components to account for dark current:

4. Dark current shot noise: The dark current shot noise variance is equal to the number of accumulated electrons, so that $\sigma_{D\_SHOT}^2 = t_e D_R$.
5. Dark current FPN: The dark current rate slightly varies between pixels, with the non-uniformity characterized by the *dark current FPN quality factor* D_N. Hence, the noise variance is given by $\sigma_{D\_FPN}^2 = t_e^2 D_R^2 D_N^2$.

Adding the listed noise components yields the noise variance for an approximately uniform, low-contrast image, which equals

$$\sigma_\eta^2 = \sigma_r^2 + (J + D_R)t_e + \left(P_N^2 J^2 + D_R^2 D_N^2\right) t_e^2. \tag{9}$$

It should be notes that an ideal camera is *shot-noise limited*, *i.e.* photon shot-noise is the only noise source that cannot be reduced by technological advances.

Noise amplification

Image deblurring by deconvolution amplifies noise, especially if the PSF $h[n]$ severely attenuates or removes certain signal components. In this section we analyze the noise amplification for inverting $h[n]$.

Convolution and deconvolution in the spatial domain are equal to multiplication and division in the frequency domain, respectively. The Discrete Time Fourier Transform (DTFT) of $h[n]$ is equal to $\mathscr{H}(e^{j\Omega})$, given by:

$$\mathscr{H}(e^{j\Omega}) = \sum_{n=-\infty}^{\infty} h[n] e^{-j\Omega n}, \tag{10}$$

$$\mathscr{H}(e^{j\Omega}) = t_e + \frac{\sin(\Delta v D T \Omega/2)}{\Delta v \cdot \sin(\Omega/2)} e^{-j\Omega \Delta v T}, \tag{11}$$

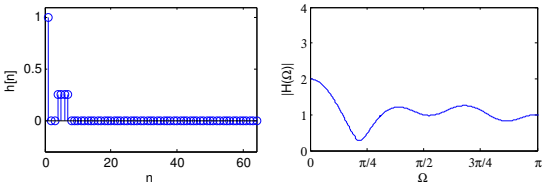

(a) One-dimensional PSF $h[n]$ (b) DTFT of PSF $\mathscr{H}(e^{j\Omega})$

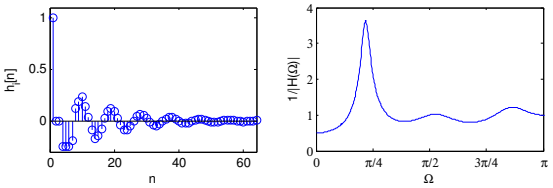

(c) Truncated inverse PSF $h_i[n]$ (d) Reciprocal of $\mathscr{H}^{-1}(e^{j\Omega})$

Figure 2: Point Spread Function $h[n]$, inverse filter $h_i[n]$ and corresponding Discrete Time Fourier Transforms

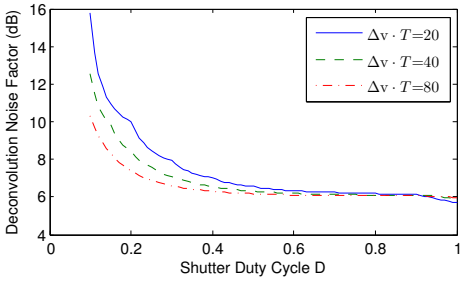

Figure 3: Deconvolution Noise Factor versus shutter duty cylce.

where $-\pi \le \Omega \le \pi$. We note that $\|\mathscr{H}(e^{j\Omega})\| > 0$ for finite values of T and Δv. Therefore, the inverse filter $h_i[n]$ exists and is defined by:

$$h_i[n] = \frac{1}{2\pi} \int_{-\pi}^{\pi} \mathscr{H}^{-1}(e^{j\Omega}) e^{j\Omega n} d\Omega. \tag{12}$$

Figures 2a to 2d illustrate $h[n]$, $\mathscr{H}(e^{j\Omega})$, $h_i[n]$ and $\mathscr{H}^{-1}(e^{j\Omega})$ for T=2.5 s, Δv=4 pixels per second and D=0.4. Although the inverse filter $h_i[n]$ has an infinite length, its response approaches zero as n approaches infinity and the filter can be truncated to a finite length.

We adopt the Deconvolution Noise Factor (DNF) [2] of $h_i[n]$ as the factor by which the signal-to-noise ratio is decreased due to deconvolution, specified by:

$$\mathrm{DNF}(h_i[n]) = \frac{\sqrt{\sum_{n=-\infty}^{\infty} \|h_i[n]\|^2}}{\sum_{n=-\infty}^{\infty} h_i[n]}. \tag{13}$$

We evaluate the DNF of $h_i[n]$ as a function of the shutter duty cycle D and the product ΔvT in Figure 3. The DNF is approximately equal to 6 dB (DNF=2) for $D \approx 1$, but is larger for smaller duty cycles. Furthermore, we observe that the DNF becomes smaller when (ΔvT) increases.

Signal to Noise Ratio

We use the Signal-to-Noise Ratio (SNR) to evaluate the image quality of the sharp image I_s. Recalling that the signal level is

DOI: 10.2352/ISSN.2470-1173.2016.18.DPMI-030

equal to It_e, the SNR in images I_1 and I_2 equals $20\log_{10}\left(It_e/\sigma_\eta\right)$. Adding I_1 and I_2 increases the SNR by a factor $\sqrt{2}$. On the other hand, deblurring decreases the SNR with the DNF, resulting in:

$$\mathrm{SNR} = 20\log_{10}\left(\frac{\sqrt{2}}{\mathrm{DNF}}\frac{It_e}{\sigma_\eta}\right). \tag{14}$$

Simulation

We compare the performance of SMIP with that of MIP [1] and Impulse Photography (IP). The parameters of the noise model are calibrated on an surveillance NOX-20 camera [1] at room temperature using the Photon Transfer Curve method [3].

Three lighting scenarios with average light intensity $J = 10^4$, $J = 10^5$ and $J = 10^6$ photon interactions per second per pixel are evaluated. With an aperture of F/5.6, quantum efficiency of 0.45, average reflectivity of 0.5 and a pixel pitch of 6.4 μm, this corresponds to 105 lux, 1050 lux and 10,500 lux, respectively. An object moves vertically with a constant speed of 1000 pixels per second. We compare the following three image capturing methods:

1. Impulse Photography limits the exposure time such that motion blur is at most 1 pixel ($t_e \leq 1$ ms). Any object moving at a speed of up to 1000 pixels per second in an arbitrary direction is captured without motion blur.
2. MIP moves the field-of-view with a constant acceleration. The velocity ranges from 0 to 1000 pixels per second, exploiting the asymmetric velocity prior, as proposed by McCloskey [8]. Any object moving at a speed between 0 and 1000 pixels along a one-dimensional motion trajectory can be deblurred during post-processing.
3. SMIP Captures two images, one without camera motion and the other with the field-of-view moving at 1000 pixels per second. Only objects moving at either 0 or 1000 pixels per second can be deblurred during post-processing.

Figures 4a to 4c depict the SNR as a function of exposure time. Whereas IP cannot extend t_e beyond 1 ms, both MIP and SMIP can increase t_e to improve the SNR. MIP is beneficial at moderate t_e, but offers little advantage at long exposures. On the other hand, SMIP is the worst performer at short to moderate exposure times, but improves significantly at long exposures. This is due to relatively low duty cycles at short exposure times, as illustrated in Figure 3.

Figures 5a to 5h are examples of a simulated scenario with a moving vehicle and a static background. The SNR of the images 5b, 5d and 5g are indicated as open dots in Figure 4a. The minor deviations of the SNR are due to the fact that the images are not low-contrast. Note that the license plate is clearly readable in Figure 5g, whereas Figures 5b and 5d are too noisy. On the other hand, erroneous motion estimation causes severe artefacts as shown in Figure 5h. Neither IP nor MIP suffer from these artefacts.

Furthermore, boundaries between the object area and the background introduce artefacts in Figure 5g. The road centerline near the license plate appears sharp in Figure 5e and is occluded by the sharp image of the vehicle in Figure 5f. The resulting image I_s in Figure 5g is a superposition of two sharp images at the motion boundary. Consequently, the inverse filter $h_i[n]$ does not match the true PSF. The boundary artefact becomes more pronounced at longer camera overhead times.

[1] Commercially available from Ampleye ltd.

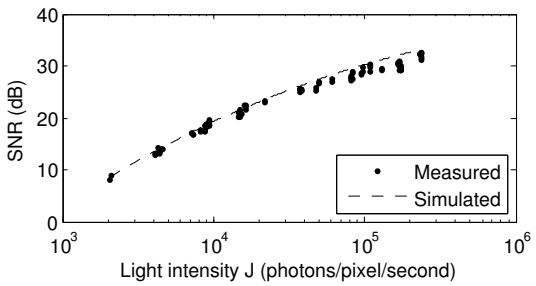

Figure 6: Simulated versus measured SNR on uniform test targets.

Experiments

We modify the image stabilization hardware inside a standard DSLR lens (EF-S 18-55 mm) equipped with image stabilization, to shift the field-of-view and verify our theoretical findings. As described in [16], a microcontroller connects to the image stabilization circuitry to control the lens shift. The lens is mounted on a NOX-20 video camera with a frame rate of 25 Hz. Note that our camera features a global shutter, which is essential to prevent rolling-shutter distortions. A digital output of the camera to the microcontroller is configured to be high if the shutter is opened. The microcontroller waits 35 ms after the shutter opens, prior to initiating the lens motion, leaving 5 ms to account for the response time of the lens. The lens quickly returns to its initial position once the shutter is closed again. We reserve 10 ms for the lens to return to its initial position, limiting the exposure time to $t_e \leq$30 ms.

We first verify our noise model by capturing and deblurring pairs of SMIP images of uniform test targets, and measure the noise level with t_e=30 ms and T=40 ms (25 Hz). An object moving at an equivalent speed of 180 pixels per second is tracked during the exposure. Figure 6 plots the measured SNR versus the simulated SNR. There is no significant difference between the measured- and simulated noise levels, giving confidence to the described noise model.

We then set up the camera to capture video of traffic driving perpendicular to the camera at a distance of 110 m. The focal distance of the lens is set to 55 mm. A laptop decodes and stores the video stream, computes the optical flow, derives the vehicle speed in pixels per second and sends it to the microcontroller. The lens velocity is alternated between background- and vehicle speed, resulting in a video sequence alternating between images having (1) a sharp background with a blurred vehicle, and (2) a blurred background with a sharp vehicle. Figure 7 depicts a challenging example with a partial occlusion due to a vehicle passing behind a tree. Whereas conventional deblurring with a static camera requires careful segmentation, SMIP allows deblurring with a single deblurring filter. The deblurred image is shown in Figure 7c. The slight ghosting artefacts near the back of the van are similar to those observed during simulations. On the other hand, the occlusions from tree branches are handled without visible artefacts.

DOI: 10.2352/ISSN.2470-1173.2016.18.DPMI-030

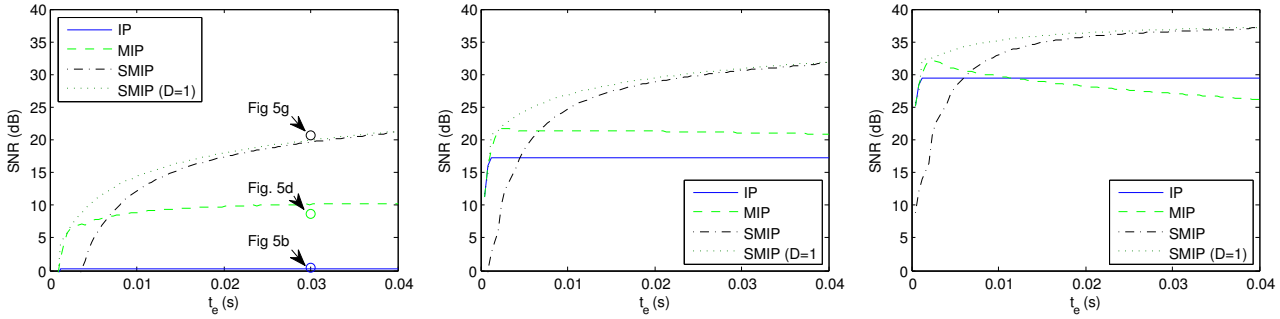

(a) $J = 10^4$ photons/pixel/second (b) $J = 10^5$ photons/pixel/second (c) $J = 10^6$ photons/pixel/second

Figure 4: Simulated SNR versus exposure time for IP, MIP [1, 8] and SMIP. The ideal SMIP case with D =1 is included for reference.

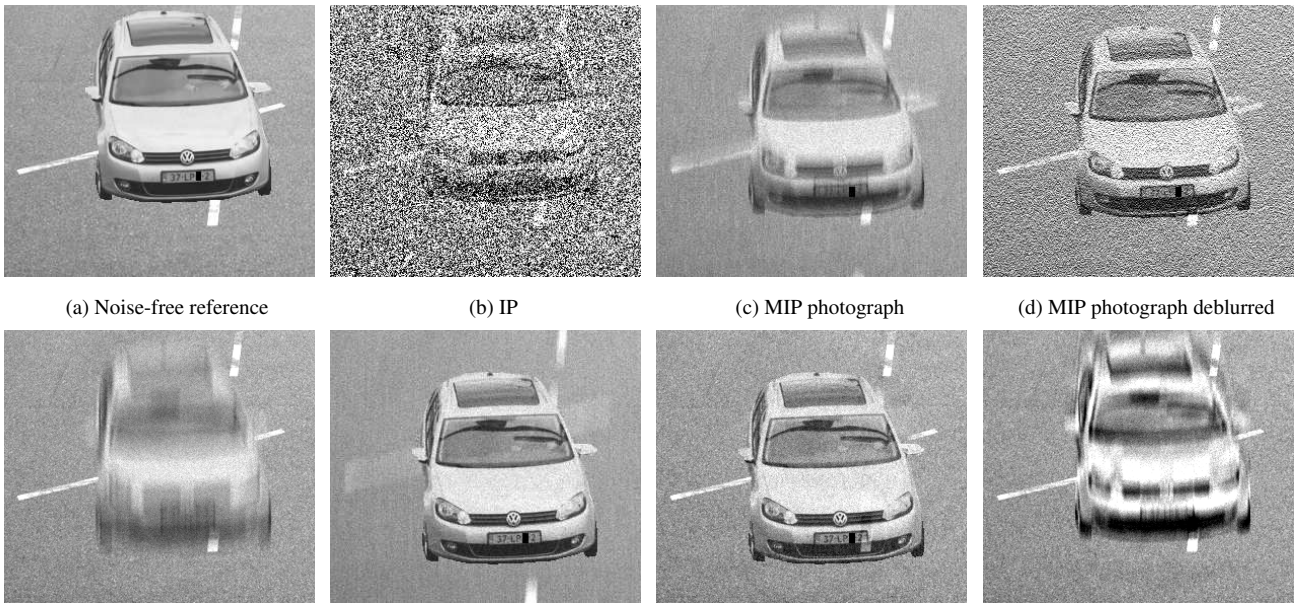

(a) Noise-free reference (b) IP (c) MIP photograph (d) MIP photograph deblurred

(e) SMIP photograph 1 (f) SMIP photograph 2 (g) SMIP added and deblurred (h) SMIP with erroneous motion prior

Figure 5: Simulations comparing (b) IP (SNR=3.2 dB), (d) MIP (SNR=12.6 dB) and (g) SMIP (SNR=20.5 dB). The exposure is normalized for comparison. Light intensity $J = 10^4$ photon interactions per second per pixel (105 lux), t_e=30 ms and T=40 ms (D=0.75). The vehicle moves at an equivalent speed of 1000 pixels per second. Figure 5h illustrates the effects of an object velocity of 500 pixels per second, while a velocity of 1000 pixels per second is assumed. (Best viewed electronically)

(a) I_1 camera tracking the vehicle. (b) I_2 camera tracking the background. (c) $I_1 + I_2$ deblurred

Figure 7: Images of vehicle moving at an equivalent speed of 1063 pixels per second (54 km/h) with t_e=30 ms and T=40 ms (D=0.75). (Best viewed electronically)

DOI: 10.2352/ISSN.2470-1173.2016.18.DPMI-030

Conclusion and future work

We have demonstrated that lens motion and prior knowledge about the motion in a scene allows for significant image quality improvement. We have proposed to capture two images in quick succession, the first while stabilizing for one velocity, while the second stabilizes for the other velocity. Next, both images are added and deblurred to produce a sharp image without the need for segmentation and local blur estimation.

We have shown that Sparse Motion-Invariant Photography (SMIP) offers a significant increase of the SNR compared to existing techniques, even when taking into account signal-dependent noise sources. Furthermore, we have demonstrated that the increased SNR results in an improved perceptual image quality, despite artefacts near the boundaries of motion areas. A disadvantage is that our method is not robust to motion estimation errors. Accurate motion estimation is necessary to prevent severe artefacts. Finally, we have shown that our solution works as expected in practice, using modified optical image stabilization hardware as an actuator. The measured SNR is in agreement with the simulation model. This simulation model was calibrated on a real camera, taking into account various realistic noise sources, which were properly modeled. The mathematical model and corresponding deblurring process are relatively simple and robust. The final image is deblurred without significant distortion.

Various topics remain for future research. First, we expect that SMIP can be applied to scenes with more than two distinct velocities, by capturing more images and coarse object segmentation. Second, with respect to robustness and deal with practical scenarios, handling saturated pixels and pulsed light sources pose interesting challenges to the algorithm. Also, the detection of erroneous motion estimation and its associated handling will make the algorithm more robust in practical situations. Third, as discussed earlier, a single-image approach is possible if motion position feedback or accurate calibration is available. The single-image approach is beneficial for cameras with a low frame rate.

Acknowledgment

The authors express their gratitude to Prodrive Technologies B.V. for providing the facilities and funding this research.

References

[1] A. Levin, P. Sand, T. S. Cho, F. Durand, and W. T. Freeman, "Motion-invariant photography," *ACM Transactions on Graphics (TOG)*, vol. 27, no. 3, p. 71, 2008.

[2] A. Agrawal and R. Raskar, "Optimal single image capture for motion deblurring," in *Computer Vision and Pattern Recognition, 2009. CVPR 2009. IEEE Conf. on*. IEEE, 2009, pp. 2560–2567.

[3] J. R. Janesick, *Photon transfer*. SPIE press San Jose, 2007.

[4] O. Cossairt, M. Gupta, and S. K. Nayar, "When does computational imaging improve performance?" *Image Processing, IEEE Transactions on*, vol. 22, no. 2, pp. 447–458, 2013.

[5] R. Raskar, A. Agrawal, and J. Tumblin, "Coded exposure photography: motion deblurring using fluttered shutter," *ACM Transactions on Graphics (TOG)*, vol. 25, no. 3, pp. 795–804, 2006.

[6] S. McCloskey, K. Muldoon, and S. Venkatesha, "Motion invariance and custom blur from lens motion," in *Computational Photography (ICCP), 2011 IEEE Int. Conf. on*. IEEE, 2011, pp. 1–8.

[7] S. McCloskey, "Improved motion invariant deblurring through motion estimation," in *Computer Vision–ECCV 2014*. Springer, 2014, pp. 75–89.

[8] S. McCloskey, K. Muldoon, and S. Venkatesha, "Motion aware motion invariance," in *Computational Photography (ICCP), 2014 IEEE Int. Conf. on*. IEEE, 2014, pp. 1–9.

[9] T. S. Cho, A. Levin, F. Durand, and W. T. Freeman, "Motion blur removal with orthogonal parabolic exposures," in *Computational Photography (ICCP), 2010 IEEE Int. Conf. on*. IEEE, 2010, pp. 1–8.

[10] A. Levin, R. Fergus, F. Durand, and W. T. Freeman, "Image and depth from a conventional camera with a coded aperture," in *ACM Transactions on Graphics (TOG)*, vol. 26, no. 3. ACM, 2007, p. 70.

[11] W. T. Cathey and E. R. Dowski, "New paradigm for imaging systems," *Applied optics*, vol. 41, no. 29, pp. 6080–6092, 2002.

[12] S. W. Hasinoff and K. N. Kutulakos, "Light-efficient photography," *Pattern Analysis and Machine Intelligence, IEEE Transactions on*, vol. 33, no. 11, pp. 2203–2214, 2011.

[13] D. Vaquero, N. Gelfand, M. Tico, K. Pulli, and M. Turk, "Generalized autofocus," in *Applications of Computer Vision (WACV), 2011 IEEE Workshop on*. IEEE, 2011, pp. 511–518.

[14] O. Cossairt and S. Nayar, "Spectral focal sweep: Extended depth of field from chromatic aberrations," in *Computational Photography (ICCP), 2010 IEEE Int. Conf. on*. IEEE, 2010, pp. 1–8.

[15] C. Zhou, D. Miau, and S. K. Nayar, "Focal sweep camera for space-time refocusing," 2012.

[16] B. Kofoed, E. Janssen, and P. H. N. de With, "Dynamic focus control for preventing motion blur," in *Advanced Video- and Signal-based Surveillance, 2015. AVSS 2015. IEEE Conf. on*. IEEE, 2015.

Author Biography

Bart Kofoed received the B.Sc. and M.Sc degrees in electrical engineering from the Eindhoven University of Technology in 2011 and 2014, respectively. Since 2014, he is pursuing the Ph.D. degree at the Video Coding and Architectures, part of the Signal Processing and Systems department of the Eindhoven University of Technology in close collaboration with Prodrive Technologies. His research primarily focuses on optimizing the low-light capabilities of camera systems, involving image capturing methods and post-processing algorithms.

Eric Janssen received the M.Sc degree in Embedded Systems from the Eindhoven University of Technology in 2012. Since 2008, he is involved with Prodrive Technologies developing high-end camera systems. First as a software engineer while later as a system architect. Currently, he is program manager of the Vision and Sensing technology program at Prodrive Technologies developing and producing solutions including safety and security cameras, medical imaging, industrial cameras.

Peter H.N. de With received the M.Sc and Ph.D. degrees from Eindhoven and Delft Universities of Technology, respectively. He has worked at Philips Research Labs Eindhoven from 1984 until 1997. He was appointed full professor at Mannheim University, Germany, between 1997 and 2000. Afterwards, he was principal consultant at LogicaCMG Eindhoven, the Netherlands, up to 2007 while simultaneously being a part-time professor at Eindhoven University of Technology, where he is now full professor. Between 2008 and 2011, he was Vice-President video technology at Cyclomedia Technology, Zaltbommel, the Netherlands. Mr. De With is (co-)recipient of various paper awards and Fellow of the IEEE.